

# Elasticity and plasticity of two-dimensional amorphous solid layers of $\beta$ -lactoglobulin

S. Courty<sup>1,a</sup>, B. Dollet<sup>1</sup>, K. Kassner<sup>2</sup>, A. Renault<sup>3</sup>, and F. Graner<sup>1,b</sup>

<sup>1</sup> Laboratoire de Spectrométrie Physique, UMR 5588 CNRS - Université J. Fourier Grenoble 1, BP 87, F-38402 Saint Martin d'Hères cedex, France

<sup>2</sup> Institut für Theoretische Physik, Otto-von-Guericke-Universität Magdeburg, Postfach 4120, D-39016 Magdeburg, Germany

<sup>3</sup> Groupe Matière Condensée et Matériaux, UMR 6626 CNRS - Université Rennes 1, Campus de Beaulieu, Bât. 11A, F-35042 Rennes cedex, France

Received 10 February 2003 and Received in final form 3 April 2003 /

Published online: 27 May 2003 – © EDP Sciences / Società Italiana di Fisica / Springer-Verlag 2003

**Abstract.** We investigate the mechanical properties of a two-dimensional amorphous solid. It is formed spontaneously by the adsorption of a protein (the  $\beta$ -lactoglobulin) at the surface of water. We measure its mechanical response in both elastic and plastic regimes by applying a point-like force (using a glass fiber). We compare our results with previous measurements of shear moduli using a floating torsion device.

**PACS.** 68.47.Pe Langmuir-Blodgett films on solids; polymers on surfaces; biological molecules on surfaces – 87.15.La Biomolecules: Mechanical properties – 62.20.Dc Elasticity, elastic constants – 62.20.Fe Deformation and plasticity (including yield, ductility, and superplasticity)

## 1 Introduction

Proteins spontaneously adsorb from aqueous solutions to the surface of water [1], essentially due to the entropy increase resulting from dehydration of the hydrophobic regions of both the interface and the protein surface [2]. The protein adsorption decreases the surface energy, slightly favoring the formation of foams and emulsions; more important, once such a dispersion is formed, its stability relies essentially on the viscoelastic properties of the protein layer, which control the rate of liquid drainage within the films, as well as film rupture [3]. This ability to form and stabilise foams and emulsions is especially important for the preparation of multiphasic aliment using food proteins [4].

$\beta$ -lactoglobulin is a protein produced in large amounts in milk. It represents a quarter of the protein fraction of bovine lactoserum. Its sequence and structure are known [5]; for a review, see [6]. Due to its high solubility in water, it is a convenient agent to form foams, emulsions and gels. It is often used after industrial treatments such as lactosylation (Maillard reaction): covalent attachment of one or several lactose molecules on the lysine residues of the protein [7].

When adsorbing to and saturating a hydrophobic surface such as air-water interface, this protein spontaneously

forms a very rigid monolayer which resists shear and is in fact a two-dimensional (2D) solid. Such a solid is amorphous, as can be checked by a Brewster-angle microscope [8] (sketched in Fig. 1). Surface shear studies have investigated how a modification of the protein properties (due, for instance, to aging or thermal treatments) affects the rheological properties of the 2D solid [9,10].

Renault and coworkers [11,12] have extensively measured the shear elastic constants of these protein layers during adsorption and solidification. They used a centimeter-size device floating on water, rotating periodically with an amplitude much smaller than 1 radian, under a sinusoidally varying magnetic driving torque, resisted by the protein layer's 2D shear elasticity to be measured [13], similar to a device invented to investigate the viscoelasticity of suspended soap films [14].

We aim at a better understanding of the interfacial mechanical properties of these proteins. More fundamentally, we also use them as examples to investigate the mechanics of 2D amorphous solids, which are still poorly understood. In this paper, we study the mechanical properties of these solid layers in a wide range of loading, from linear elasticity to large plastic deformation. We perform measurements at the scale of 10  $\mu\text{m}$ , and compare them with those of Renault *et al.* at a scale a thousand times larger.

We use a soft glass fiber to both apply a force on the layer, and measure it. The principle of our experimental set-up is similar to the one developed by Barentin *et al.* [15,16] to measure the surface viscosity of a monolayer:

<sup>a</sup> Present address: Cavendish Laboratory, Madingley Road, Cambridge, CB3 0HE, UK; e-mail: sc374@phy.cam.ac.uk

<sup>b</sup> e-mail: graner@ujf-grenoble.fr

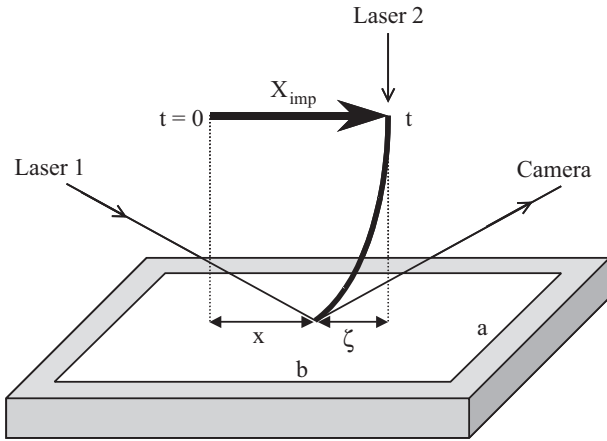


**Fig. 1.** Experimental set-up. A Brewster-angle microscope (sketched here as a laser 1 hitting the surface at Brewster angle, and camera) monitors the protein layer while a soft fiber (which guides the laser 2) simultaneously deforms it.

we determine the horizontal force between the monolayer and a round obstacle moving with respect to each other. However, since in the case of viscosity the coupling with the 3D phase suppresses the long-range divergences which do exist in 2D elasticity, our calculations are different from theirs.

## 2 Materials and methods

### 2.1 Preparation of protein layer

The  $\beta$ -lactoglobulin is a generous gift from S. Bouhalab (Laboratoire de Recherches de Technologie Laitière, INRA, Rennes) who purified it according to the protocol explained in [7], either as native protein, or after a lactosylation treatment in powder (lac130) or in solution (DW-lac6). The proteins are lyophilised and stored at 4 °C. Before deposition, they are dissolved at concentration 5  $\mu$ g/ml in a phosphate buffer (sodium phosphate 0.1 M, NaCl 0.1 M, pH 6.8  $\pm$  0.1).

The trough is 8 cm long, 2 cm wide, and 0.7 cm deep. Its sides are made of teflon (PTFE), its bottom is a glass plate which allows for the transmission of the laser beam for force measurement, as explained below. All experiments are realized at room temperature, 20.5 °C. We define the age  $A$  of the protein layer with reference to the moment, referred to as  $A = 0$ , where the protein is injected in the trough; this is less than 15 minutes after the preparation of the protein solution. Measurements begin while and after the proteins adsorb at the surface of water.

### 2.2 Force sensor: soft optical fiber

We use a vertical glass fiber (Fig. 1), actually a denuded optical fiber (Thorlabs). Its free end crosses the protein layer and immerses 10  $\mu$ m below the surface. We silanise

the fiber (*n*-octadecyltrichlorosilane diluted at 2% in octane): we obtain a contact angle close to 90 °, as checked with a camera attached to the side of the trough; this results in a meniscus of at most a few microns, as estimated with the Brewster-angle microscope.

The fiber is held in a concentric chuck (Melles-Griot) fixed on a horizontal translation stage (M-UMR5, Microcontrole) with a micrometric thrust coupled to a step-by-step motor (Stebon, 400 steps/turn), allowing for a horizontal imposed displacement  $X_{\text{imp}}$  up to 6 mm. Thus, the fiber applies a horizontal point-like deformation to the protein layer.

We then measure the horizontal displacement  $\zeta$  of the free end of the fiber with respect to its fixed end. We can deduce the horizontal force  $F$  exerted by the protein layer on the vertical fiber, through the equation  $F = K\zeta$ : here  $K$  is the bending rigidity of the fiber, which needs to be determined (see below).

We finally deduce the resistance of the protein layer, that is, the effective layer rigidity  $k_{\text{eff}}$ , defined as the ratio of the force  $F$  to the horizontal displacement  $X = X_{\text{imp}} - \zeta$  of the fiber within the protein layer:

$$k_{\text{eff}} = \frac{F}{X} = \frac{K\zeta}{X_{\text{imp}} - \zeta}. \quad (1)$$

As long as the solid layer remains in its linear elastic regime,  $k_{\text{eff}}$  remains constant. It is a global property of the whole solid (its material, its size, and geometry) under a given applied deformation. In fact,  $k_{\text{eff}}$  represents a physically intuitive quantity: the rigidity one would feel by sticking a finger in the solid and moving it laterally.

To measure the deflection  $\zeta$  of the fiber, we connect it to a laser (“Laser 2” in Fig. 1) consisting of a diode (Melles-Griot, 10 mW, 632.88 nm). Its diverging beam crosses the glass bottom of the trough and reaches below the trough a photodetector (Position Sensing Detector, Radiospares) fixed onto the same translation stage as the fiber itself. The signal of the detector, recorded on the computer through a DAC card, measures (up to a known factor) the actual deflection  $\zeta$ .

To calibrate the bending rigidity  $K$  of the fiber, we hold the fiber horizontally and measure with a camera its deflection under its own weight (for low  $K$ ) or under added weights (for high  $K$ ). The fiber deflection, both linear and reversible, is elastic. The rigidity  $K$  of a fiber of radius  $r$  and length  $L$  goes like  $K \sim r^4/L^3$  [17]. It is easy to vary it over several orders of magnitude by adjusting: either  $r$ , by attacking the glass with fluorhydric acid at 40% concentration; or  $L$ , by changing the height of the chuck above the water surface.

We have studied the same protein layer using fibers with different rigidities ranging from 0.3 to 33 mN/m. As expected, with all fibers we measure the same effective protein layer rigidity  $k_{\text{eff}}$ , namely  $1 \pm 0.1$  mN/m. As expected, again, we obtain the best signal/noise ratio when  $\zeta$  and  $X = X_{\text{imp}} - \zeta$  are both large, that is (Eq. (1)), when the fiber rigidity is comparable to the protein layer rigidity (data not shown, see Ref. [18], pp. 44 and 132). To perform the measurements we report below, we use a

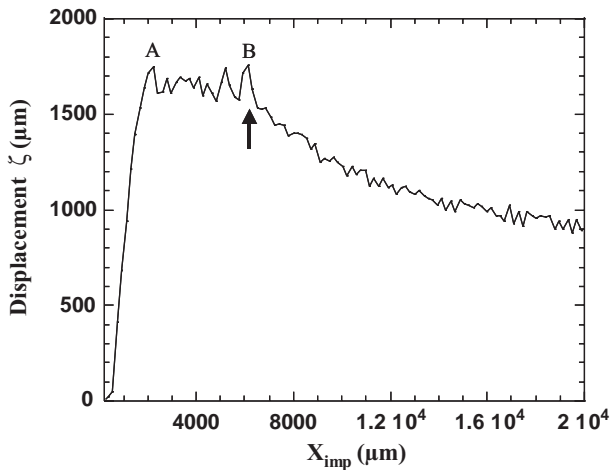


**Fig. 2.** Example of experimental measurement of the deflection  $\zeta$  of the fiber, hence of the force  $F = K\zeta$ , versus the displacement  $X$  of the fiber lower end. It represents the mechanical response of the 2D solid, while the fiber is displaced at speed  $\dot{X}_{\text{imp}} = 372 \mu\text{m s}^{-1}$ . *A*: yield point. *B* (arrow): the fiber is stopped ( $\dot{X}_{\text{imp}}$  is set to 0) and the relaxation begins.

fiber of diameter  $2r = 26 \pm 1 \mu\text{m}$ , length  $L = 1.5 \pm 0.1 \text{ cm}$ , rigidity  $K = 1.64 \pm 0.08 \text{ mN/m}$ .

### 2.3 Mechanical measurements

We move the fiber at constant applied velocity  $\dot{X}_{\text{imp}}$  chosen between 25 and  $2500 \mu\text{m s}^{-1}$ . We have checked that, in the absence of the protein layer, the force exerted by the pure water is too low to be measurable (data not shown).

Figure (2) presents a typical recording and evidences three phases:

- The elastic regime. After a short waiting time, the force increases linearly with time  $t$ , until point *A*.
- (*A-B*): the plastic regime. The protein layer yields, then the force reaches a plateau  $F_p$ .
- From point *B* onwards, a relaxation phase.

From such force recording we measure directly the plateau force  $F_p$  as an average over  $F(t) = K\zeta(t)$  on the plateau (*A-B*). On the other hand, it is more indirect to extract the elastic properties, for the following reasons.

In linear elasticity, the elastic moduli of an amorphous (hence isotropic) 2D solid are characterized by two numbers, for instance its shear modulus  $\mu$  and its Poisson coefficient  $\nu$ . They are defined by the Hooke's law, that is, the relation between the stress tensor  $\sigma$  and the strain tensor  $u$  [17]. In the present case, where the stress has no vertical diagonal component ("plane stress",  $\sigma_{zz} = 0$ ), the 2D Hooke's law writes

$$\begin{aligned} \sigma_{xx} + \sigma_{yy} &= 2\mu \frac{1+\nu}{1-\nu} (u_{xx} + u_{yy}), \\ \sigma_{xx} - \sigma_{yy} &= 2\mu (u_{xx} - u_{yy}), \\ \sigma_{xy} &= 2\mu u_{xy}. \end{aligned} \quad (2)$$

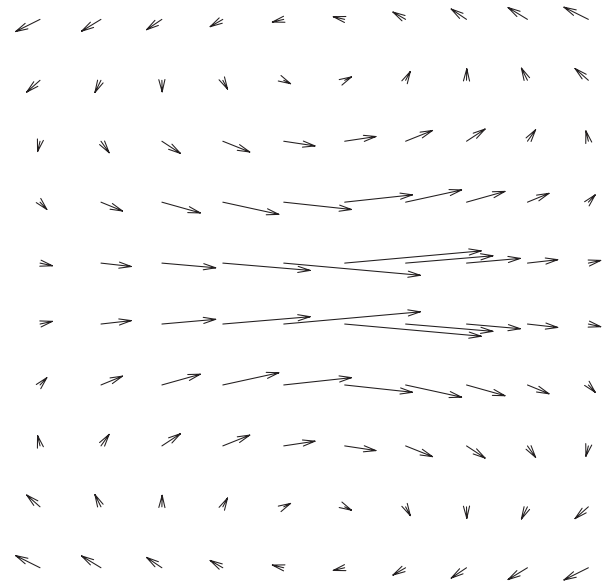


**Fig. 3.** Displacement field  $\mathbf{u}(x, y)$  within the 2D solid, for a force exerted towards the right by a fiber in the center (not drawn). This plot has been calculated up to  $\mathcal{O}(r/a, r/b)$  terms, in the case of square geometry ( $a = b$ ), no-slip boundary conditions ( $\mathbf{u}$  vanishes at the boundaries) and  $\nu = 0$ .

From a linear fit of the  $F(t) = K\zeta(t)$  curve in the elastic regime, we measure the slope  $\dot{\zeta}$ . We then deduce the effective rigidity  $k_{\text{eff}}$  of the protein layer (Eq. (1)) through

$$k_{\text{eff}} = \frac{dF}{dx} = \frac{K \dot{\zeta}}{\dot{X}_{\text{imp}} - \dot{\zeta}}. \quad (3)$$

What information can we extract from  $k_{\text{eff}}$ ? Obviously,  $k_{\text{eff}}$  is a function of  $\mu$  and  $\nu$ . Can we calculate this function? This is far from trivial, due to the long range of elastic interactions in 2D.

In the appendix we calculate the deformation field induced by the fiber in the 2D solid for the geometry of our experimental set-up. We must specify the boundary conditions: whether the monolayer is anchored, or not, to the boundaries will affect the respective importance of compression and shear induced by the fiber. Since we do not have access to this information, we chose for simplicity to solve the no-slip boundary conditions. We note that the results of our calculations (Fig. 3) look similar to our observations of the displacement of beads inserted in the layer (data not shown).

From these calculations, we deduce the relation between the effective rigidity and the shear modulus (Eq. (A.6)):

$$\frac{\mu}{k_{\text{eff}}} = 1.067 - 0.329 \nu. \quad (4)$$

Hence,  $\mu$  is very close to the measured value  $k_{\text{eff}}$ , with a small correction which depends on the value of  $\nu$ .

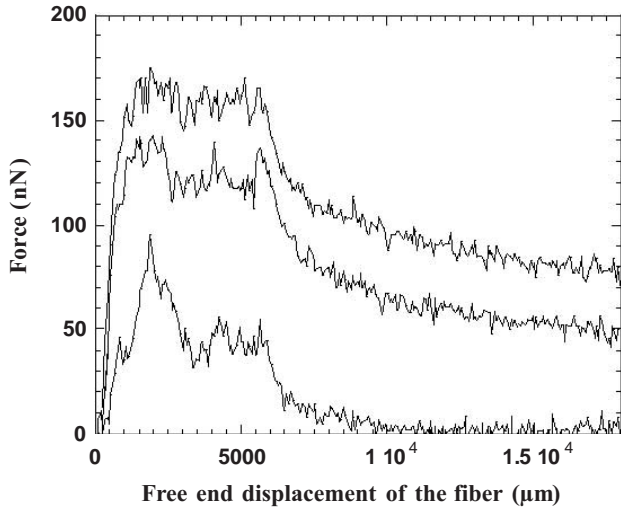


**Fig. 4.** Formation and solidification of the native protein layer: force displacement curve  $F(X)$  at different ages  $A$  after protein injection. From bottom to top:  $A = 0.78, 4.25$  and  $6.21$  hours. The fiber velocity is  $\dot{X}_{\text{imp}} = 123 \mu\text{m s}^{-1}$  for each curve.

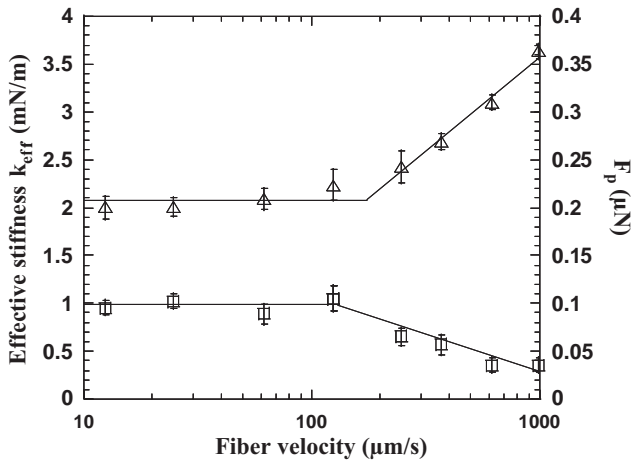


**Fig. 5.** Variations of  $k_{\text{eff}}$  (squares, left scale) and  $F_p$  (triangles, right scale) with the fiber velocity  $\dot{X}_{\text{imp}}$ . The horizontal lines indicate the average of low-velocity data; the tilted lines are linear fits of high-velocity data. Their intersections determine the critical velocity  $\dot{X}_c$ . We find  $\dot{X}_c = 110 \pm 25 \mu\text{m s}^{-1}$ . Here the age of the layer is  $A = 8$  hours. Note the semi-logarithmic scale.

### 3 Results

#### 3.1 Solidification of the 2D $\beta$ -lactoglobulin layer

We have followed the formation of the 2D  $\beta$ -lactoglobulin solid at successive ages, after protein injection (Fig. 4). Both the effective stiffness  $k_{\text{eff}}$  and the plateau force  $F_p$  increase with the age of the protein layer, reflecting its progressive solidification.

#### 3.2 Elasticity of the 2D $\beta$ -lactoglobulin solid

Figure 5 presents measurements performed after 8 hours, when the protein layer rigidity does not seem to evolve

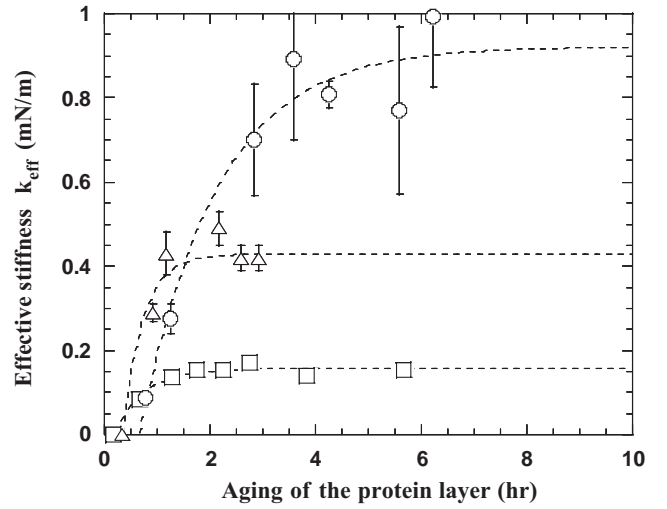


**Fig. 6.** Comparison between the effective stiffness of the  $\beta$ -lactoglobulin (circles), the DW-lac6 (squares), and the lac130 (triangles). Measurements are performed at  $\dot{X}_{\text{imp}} = 123 \mu\text{m s}^{-1}$ . Dotted lines are guides for the eye.

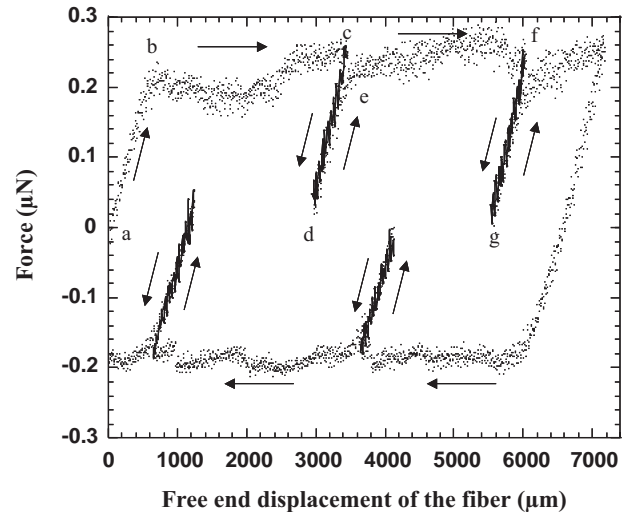


**Fig. 7.** Cycles of loading ( $a-c, d-f, \dots$ ) and unloading ( $c-d, f-g, \dots$ ) in a 2D  $\beta$ -lactoglobulin solid in plastic regime. Letters  $b, e, \dots$  correspond to yield points.

any longer (as already observed in Ref. [11]). It shows that, at low velocity  $\dot{X}_{\text{imp}}$  the values of  $k_{\text{eff}}$  and  $F_p$  are independent of  $\dot{X}_{\text{imp}}$ . Above  $\dot{X}_c$ , the velocity-dependent dissipation becomes high enough to progressively affect the mechanical response of the protein layer. We thus perform the following measurements for  $\dot{X}_{\text{imp}} = 123 \mu\text{m s}^{-1}$ , in the cross-over region. We find that the  $\beta$ -lactoglobulin is significantly stiffer than its two treated variants (Fig. 6).

#### 3.3 Plastic behaviour of the 2D $\beta$ -lactoglobulin solid

In the plastic regime, Figure 7 displays cycles of loading and unloading. In  $a-b$ , the layer responds elastically. It yields in  $b$ ; from  $b$  to  $c$  it covers a plastic plateau,

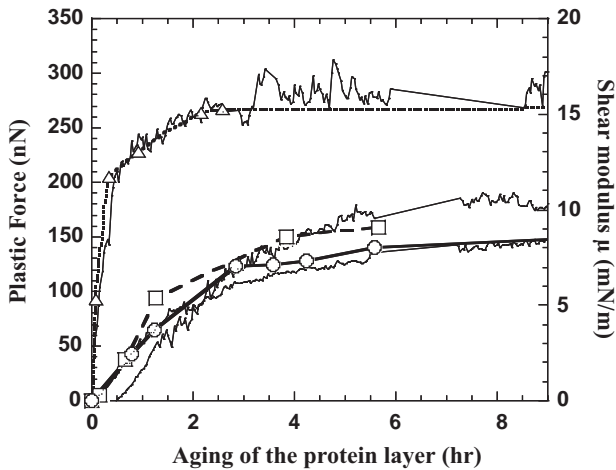


**Fig. 8.** Aging of the protein layer: comparison between the plastic force measured here with the fiber (symbols, left scale), and the shear modulus measured by torsion [11] (lines, right scale). Legend:  $\beta$ -lactoglobulin (circles, solid line); DW-lac6 (squares, dashed line); and lac130 (triangles, dots).

with a roughly constant force. Points *b* and *c* are completely equivalent from the macroscopic point of view, although they are microscopically different (as two microscopic states of a gas differ). However, by unloading at *c* and re-loading at *d*, we observe that the layer behaves elastically and reversibly. This reversibility is repeatedly observed, for instance at *f*. This does not depend on the sign of the loading, as is clear from the lower part (negative forces) of Figure 7.

Moreover, by collapsing all loading and unloading curves, we observe that they all have the same slope within 10% (not shown). Hence, all these different microscopic states *b*, *c*, *e*, *f*, have the same effective stiffness.

The plastic force increases with the age of the protein layer (Fig. 8). Surprisingly, this increase seems to parallel that of the shear modulus measured by the torsion method [11]: see discussion.

## 4 Discussion, conclusion and perspectives

We have investigated a monolayer of  $\beta$ -lactoglobulin at the surface of water which spontaneously forms an amorphous 2D solid. We have measured its rheological response under a point-like force, using a soft fiber.

Our results concern four points:

- i) *The elastic, plastic and viscous behaviours.* We have followed the solidification of the protein layer. When the solid is formed, we measure its effective stiffness  $k_{\text{eff}}$  and the plateau force  $F_p$ . Their values are independent of the fiber velocity  $\dot{X}_{\text{imp}}$ , until  $\dot{X}_{\text{imp}}$  reaches a critical velocity  $\dot{X}_c$ , where the velocity-dependent dissipation becomes significant. We have measured  $\dot{X}_c = 110 \pm 25 \text{ } \mu\text{m s}^{-1}$ .

- ii) *The link between elastic and plastic properties.* During cycles of loading and unloading, we have observed that the elastic properties of the  $\beta$ -lactoglobulin 2D solid remain basically unchanged (with respect to the undeformed solid), even far in the plastic regime. This would suggest that the solid keeps the same statistical properties even in microscopically very different configurations.

- iii) *The comparison with torsion devices.* Our measurements of the shear modulus  $\mu$  (Fig. 6) are an order of magnitude smaller than the values obtained by Gauthier *et al.* [11] (Fig. 8, right scale). We can suggest three explanations to this discrepancy.

First, the dependence of the elastic properties on the scale of the measurement. Our measurements are performed at the scale of  $10 \text{ } \mu\text{m}$ , while torsion measurements are performed at the centimeter scale. The observed differences in order of magnitude could then reflect a heterogeneity of the 2D solid. This is compatible with what Zakri *et al.* found on solid alcohol monolayers: taking advantage of their crystalline order, they could measure values corresponding to a truly homogeneous 2D solid (by X-rays probing the intermolecular interaction potential), and found that they were orders of magnitude larger than their measurements with the torsion device [13]. Future studies might aim at better understanding the role of spatial heterogeneity on the macroscopical rheological properties, including dissipation.

Second, the mixing between elastic and plastic measurements. The fiber method unambiguously separates both regimes (Fig. 2). On the other hand, the torsion measurements (shear modulus  $\mu$ ) seem to be much more correlated to our plastic (plateau force  $F_p$ ) than elastic (effective stiffness  $k_{\text{eff}}$ ) measurements (Fig. 8). Third, the long range of elastic interactions. The ratio  $F_p/\mu$  is approximately constant and equal to  $1.75 \text{ cm}$ . This length might be characteristic of the geometry of the experimental set-ups. The present work thus suggests to revisit experiments with torsion devices; a systematic study is in progress, and preliminary results indeed indicate that the torsion devices are sensitive to the size of the trough.

- iv) *Calculations of 2D elasticity.* In the course of this study, we have calculated the macroscopic response to an in-plane external force of a 2D solid, of given elastic properties (shear modulus  $\mu$  and Poisson coefficient  $\nu$ ). Due to the logarithmic range of 2D elasticity fields, this calculation turns out to be non-trivial and involves the geometrical details of the experimental set-up. In Appendix A, we present the results, firstly using expressions as general as possible, then the particular case of our set-up. We show that the effective stiffness  $k_{\text{eff}}$  is almost equal to the shear modulus  $\mu$  (Eq. (4)).

We thank warmly S. Bouhallab for providing us with purified proteins; F. Gauthier and P. Ballet for help with experiments; F. Gauthier and J.-F. Legrand for numerous discussions; and S. Cox for reading the manuscript.

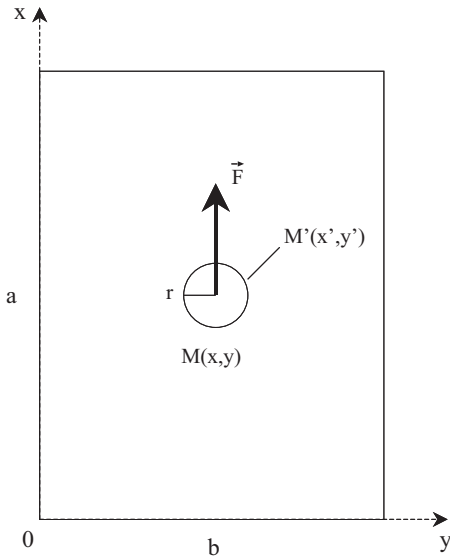


**Fig. 9.** Sketch of our experiment: the fibre (circle of radius  $r$ ) is much smaller than the trough (rectangle, sides  $a \times b$ ) in which the 2D solid is grown,  $r \ll a, b$ .

## Appendix A.

### Appendix A.1. Problem under consideration

Consider an isotropic 2D solid with given elastic properties: shear modulus  $\mu$  and Poisson coefficient  $\nu$ . An object is inserted in this solid, then displaced in-plane within the solid by a distance  $X$ . The solid deforms: a point of the solid at position  $(x, y)$  undergoes a displacement  $\mathbf{u}(x, y)$ . Due to its elastic properties, the solid resists this deformation: it applies to this obstacle a force  $\mathbf{F}$ . We want to determine  $X$  and  $|\mathbf{F}|$ , that is the effective stiffness of the solid,  $k_{\text{eff}} = |\mathbf{F}|/X$  (Eq. (1)).

The displacement field involves a recirculation: a compression in front of the obstacle, a shear on its sides, and an extension behind it (Fig. 3). Both  $\mu$  and  $\nu$  should thus enter in the expression of  $k_{\text{eff}}$ . Due to their logarithmic range, 2D elasticity fields feel the boundary conditions of the system: the expression of  $k_{\text{eff}}$  should thus also depend on the geometrical details of the experimental set-up, including the shape and size of the solid itself and of the obstacle.

### Appendix A.2. Notations

The fiber is a vertical cylinder. Its intersection with the horizontal solid, grown at the water surface in a rectangular trough, is a circle (Fig. 9). We thus model our experiment by a circular 2D obstacle. We call  $x$  its axis of displacement,  $y$  the perpendicular axis. We call  $a = 2 \pm 0.05$  cm and  $b = 8 \pm 0.05$  cm the dimensions of the trough,  $r = 13 \pm 0.5$   $\mu\text{m}$  the radius of the circle.

The origin  $O$  of the axes is at the corner of the trough, so that the obstacle is centered at position  $(a/2, b/2)$ . We denote by  $(x, y)$  the position on the surface  $S$  of the 2D

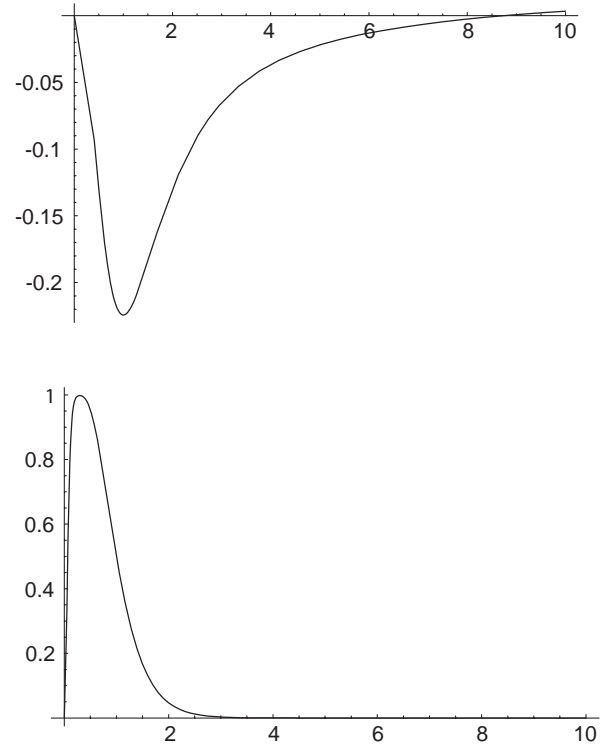


**Fig. 10.** Graph of  $f(\eta)$  and  $g(\eta)$  from equations (A.5).

solid, and by  $(x', y')$  the position on the surface  $\Sigma$  of the 2D obstacle.

Let  $\mathbf{f}$  be the force per unit surface applied by the obstacle; hence,  $-\mathbf{f}$  is the force per unit surface applied by the solid layer to the obstacle. The displacement field  $\mathbf{u}$  of the solid is given by the 2D propagator  $\overline{\overline{G}}$  defined as

$$\mathbf{u}(x, y) = -\frac{1}{\mu} \iint_{\Sigma} \overline{\overline{G}}(x, y, x', y') \cdot \mathbf{f}(x', y') \, dx' dy'. \quad (\text{A.1})$$

The effective stiffness  $k_{\text{eff}}$  is defined as the ratio of the total force applied by the fiber along axis  $x$  to the fiber displacement along  $x$  (Eq. (1)). We thus obtain it from the  $xx$ -component of  $\overline{\overline{G}}$ , or more precisely its average over the circle delimiting the obstacle,

$$\frac{\mu}{k_{\text{eff}}} = -\langle G_{xx} \rangle. \quad (\text{A.2})$$

We must take into account the finite radius  $r$  of the obstacle, since  $G_{xx}$  diverges in the limit  $r \rightarrow 0$ . Since there are also long-range divergence, we must specify the boundary conditions; as mentioned above, we chose the no-slip boundary conditions  $\mathbf{u} = \mathbf{0}$  which lead to easier calculations of the Green function.

### Appendix A.3. Propagator $\overline{\overline{G}}$ : $xx$ -component

To calculate this propagator, we need to consider images of the obstacle mirrored by each side of the rectangular box. There are thus an infinite number of reflections. The

propagator hence appears as an infinite series of terms labelled by the integer numbers  $m, n$ , namely the number of reflections on each side.

We use here the equations of 2D elasticity of continuous media, equations (2). We obtain the propagator for an infinite two-dimensional medium from the known one of the three-dimensional case by an appropriate integration along one coordinate, dropping divergent constants in the process. Once the Green's function for the infinite medium has been found (and verified by insertion into the Lamé equations with a  $\delta$ -function inhomogeneity), the propagator for a rectangle with zero displacement boundary conditions on its sides can be obtained by the method of images. This is a standard step which nevertheless requires some patience in writing as well as care to avoid divergent sums. The result is

$$G_{xx} = \frac{1+\nu}{8\pi} \sum_{m,n} \left\{ \frac{3-\nu}{2(1+\nu)} \times \ln \left( \frac{[(x-x'-2na)^2 + (y-y'-2mb)^2]}{[(x-x'-2na)^2 + (y+y'-2mb)^2]} \right) \times \frac{[(x+x'-2na)^2 + (y+y'-2mb)^2]}{[(x+x'-2na)^2 + (y-y'-2mb)^2]} \right. \\ \left. - \frac{(x-x'-2na)^2}{(x-x'-2na)^2 + (y-y'-2mb)^2} + \frac{(x-x'-2na)^2}{(x-x'-2na)^2 + (y+y'-2mb)^2} + \frac{(x+x'-2na)^2}{(x+x'-2na)^2 + (y-y'-2mb)^2} \right. \\ \left. - \frac{(x+x'-2na)^2}{(x+x'-2na)^2 + (y+y'-2mb)^2} \right\}. \quad (\text{A.3})$$

We do not need to truncate these infinite sums, which are evaluated numerically.

As a by-product of this calculation, we also obtain the  $xy$ -component of the propagator. It does not have any diverging logarithmic term, and its first  $\mathcal{O}(r/a, r/b)$  terms also vanish. This enables us to plot the displacement field  $\mathbf{u}(x, y)$  in the 2D solid, near the fiber (Fig. 3).

#### Appendix A.4. Effective stiffness $k_{\text{eff}}$

The ratio  $\mu/k_{\text{eff}}$  (Eq. (A.2)) depends on two geometrical parameters, the ratio  $r/b$  of the fiber radius to the trough width, and the trough aspect ratio  $\eta = a/b$ , according to the expression

$$\frac{\mu}{k_{\text{eff}}} = -\frac{3-\nu}{16\pi} \left[ 2 \ln \frac{r}{b} + 4 \ln \coth \frac{\pi\eta}{2} - \ln(1+\eta^2) + f(\eta) \right] \\ + \frac{1+\nu}{8\pi} \left[ \frac{1}{2} + g(\eta) \right] + \mathcal{O}(r/a, r/b), \quad (\text{A.4})$$

where

$$f(\eta) = \sum_{(m,n) \in (\mathbf{Z}^*)^2} \ln \left\{ \frac{[4\eta^2 n^2 + 4m^2][\eta^2(2n-1)^2 + (2m-1)^2]}{[\eta^2(2n-1)^2 + 4m^2][4\eta^2 n^2 + (2m-1)^2]} \right\}, \\ g(\eta) = \sum_{q \in \mathbf{Z}^*} (-1)^{q+1} \frac{\pi q \eta}{\sinh \pi q \eta}. \quad (\text{A.5})$$

Numerical summations of  $f$  and  $g$  converge quickly, and sums up to  $m^2 + n^2 \leq 100$  (for  $f$ ) and  $|q| \leq 10$  (for  $g$ ) yield a  $10^{-3}$  precision, plotted in Figure 10.

Here, for  $r = 13 \mu\text{m}$ ,  $a = 8 \text{ cm}$  and  $b = 2 \text{ cm}$ , we obtain  $f = -0.224$  and  $g = -0.500$ , yielding:

$$\frac{\mu}{k_{\text{eff}}} = 1.067 - 0.329 \nu. \quad (\text{A.6})$$

## References

1. P. Walstra, A.L. De Roos, *Food Rev. Int.* **9**, 503 (1993).
2. E. Dickinson, *J. Chem. Soc. Faraday Trans.* **94**, 1657 (1998).
3. J.-F. Sadoc, N. Rivier, *Foams and Emulsions, Proceedings of Cargese 1997 Summer School, Nato ASI Series E* (Kluwer, Dordrecht, 1999).
4. E. Dickinson, *Les Colloïdes Alimentaires* (Masson, Paris, 1996).
5. S. Brownlow, Morais J.H. Cabral, R. Cooper, D.R. Flower, S.J. Yewdall, I. Polikarpov, A.C.T. North, L. Sawyer, *Structure* **5**, 481 (1997).
6. P. Cayot, D. Lorient, in *Structures et Technofonctions des Protéines du Lait* (Arilait Recherches, Editions Technique et Documentation, Paris, 1998).
7. F. Morgan, J. Léonil, D. Mollé, S. Bouhallab, *J. Agric. Food Chem.* **47**, 83 (1999).
8. S. Henon, J. Meunier, *Rev. Sci. Instrum.* **62**, 936 (1993).
9. S. Roth, B.S. Murray, E. Dickinson, *J. Agric. Food Chem.* **48**, 1491 (2000).
10. J. Kragel, D.O. Grigoriev, A.V. Makievski, R. Miller, V.B. Fainerman, P.J. Wilde, R. Wustneck, *Colloids Surf. B* **12**, 3 (1999).
11. F. Gauthier, S. Bouhallab, A. Renault, *Colloids Surf. B* **21**, 37 (2001).
12. A. Renault, S. Pezennec, F. Gauthier, V. Vié, B. Desbat, *Langmuir* **18**, 6887 (2002).
13. C. Zakri, A. Renault, B. Berge, *Physica B* **248**, 208 (1998).
14. F. Bouchama, J.M. di Meglio, *J. Phys. Condens. Matter* **8**, 9525 (1996).
15. C. Barentin, C. Ybert, J.-M. di Meglio, J.-F. Joanny, *J. Fluid Mech.* **397**, 331 (1999).
16. C. Barentin, P. Muller, C. Ybert, J.-F. Joanny, J.-M. di Meglio, *Eur. Phys. J. E* **2**, 153 (2000).
17. L.D. Landau, E.M. Lifschitz, *Theory of Elasticity* (Reed Educational and Professional Publishing, Oxford, 1986) 3rd edition.
18. S. Courty, *Solides bidimensionnels à l'interface air-eau: mesures mécaniques et optiques*, PhD Thesis (University of Grenoble, France, 2001) unpublished. Available as .pdf file (16 Mo) at <http://www-lsp.ujf-grenoble.fr/link/courty.htm>.